Agitation in a Microcarrier-based Spinner Flask Bioreactor Modulates Homeostasis of Human Mesenchymal Stem Cells

Richard Jeske[1,#], Shaquille Lewis[1,#,a], Ang-chen Tsai[1,a], Kevin Sanders[1], Chang Liu[1], Xuegang Yuan[1,2,*], Yan Li[1,*]

1. Department of Chemical and Biomedical Engineering, FAMU-FSU College of Engineering, Florida State University, Tallahassee, Florida, United States
2. The National High Magnetic Field Laboratory, Florida State University, Tallahassee, Florida.

co-first authors

Running title: Human Mesenchymal Stem Cells in a Microcarrier-based Bioreactor

*Corresponding authors:

Dr. Yan Li: address: 2525 Pottsdamer St., Tallahassee, FL 32310, USA, Tel: 850-410-6320; Fax: 850-410-6150; email: yli4@fsu.edu.

Dr. Xuegang Yuan: xy13b@my.fsu.edu.

Contact information for others:

Richard Jeske: rjj15@my.fsu.edu

Shaquille Lewis: shaquille1.lewis@famu.edu. [a]Current address: Meharry Medical College, Nashville, TN.

Dr. Ang-chen Tsai: at11h@my.fsu.edu. [a]Current address: University of Florida, Gainesville, FL.

Kevin Sanders: kts16@my.fsu.edu. Chang Liu: cl20ev@my.fsu.edu

Submitted to *Biochemical Engineering Journal*

Abstract:

Human mesenchymal stem cells (hMSCs) are well known in cell therapy due to their secretion of trophic factors, multipotent differentiation potential, and ability for self-renewal. As a result, the number of clinical trials has been steadily increasing over the last decade highlighting the need for in vitro systems capable of producing large quantities of cells to meet growing demands. However, hMSCs are highly sensitive to microenvironment conditions, including shear stress caused by dynamic bioreactor systems, and can lead to alteration of cellular homeostasis. In this study, hMSCs were expanded on microcarriers within a 125 mL spinner flask bioreactor system. Our results demonstrate a three-fold expansion over seven days. Furthermore, our results show that culturing hMSCs in the microcarrier-based suspension bioreactor (compared to static planar culture) results in smaller cell size and higher levels of reactive oxidative species (ROS) and ROS regulator Sirtuin-3, which have implications on the nicotinamide adenine dinucleotide metabolic pathway and metabolic homeostasis. In addition, hMSCs in the bioreactor showed the increased Prostaglandin E_2 secretion as well as reduced the Indoleamine-pyrrole 2,3-dioxygenase secretion upon stimulus with interferon gamma. The results of this study provide understanding of potential hMSC physiology alterations impacted by bioreactor microenvironment during scalable production of hMSCs for biomanufacturing and clinical trials.

Key words: Human mesenchymal stem cells, shear stress, microcarrier, suspension bioreactor, metabolism

1. Introduction

Over the last quarter century, interest in human mesenchymal stem cell (hMSC) research has accelerated due to their potential in regenerative medicine, tissue engineering, and cell-based therapies. hMSCs exhibit a broad range of attractive properties such as multi-potent differentiation ability [1], secretion of cytokines to support cell survival, regulation of immune response [2], and hypo-immunogenicity [3]. Promising preclinical results have led to a major increase in clinical trials over the last decade with currently over 1,100 trials for hMSCs listed on clinicaltrials.gov for treating diseases such as graft versus host disease, diabetes, myocardial infraction, etc. hMSCs can be isolated from several tissue sources such as bone marrow, adipose tissue, dental pulp, and umbilical cord. Although majority of studies focus primarily on bone marrow-derived hMSCs, adipose tissue-derived hMSCs appear to be a promising alternative and have a higher isolation yield [4-7]. Regardless of tissue source, hMSC yields are orders of magnitude lower than the minimum effective intravenous dosage of 70-190 million cells used in clinical trials [8]. Therefore, large scale *in vitro* expansion is necessary to supply sufficient cell numbers. Furthermore, as stem cell products transcend the experimental stage and become viable commercial products, the *in vitro* expansion systems need to be scaled up under current good manufacturing practices.

One system showing potential for scale up production of hMSCs while still retaining stem cell properties is the microcarrier-based suspension bioreactors [9-12]. Lawson et. al. recently demonstrated a 43-fold expansion of hMSCs in a 50 L stirred tank bioreactor, while still retaining tri-lineage differentiation potential, surface marker expression, and capacity to modulate immune response demonstrated by their ability to suppress T cell proliferation via Indoleamine 2,3-dioxygenase (IDO) induction [9-12]. Suspension bioreactors are able to achieve high levels of expansion due to high surface area to volume ratio. As hMSCs are an adherent cell type, proliferation is directly affected by available surface area. Within the suspension bioreactors, microcarriers are suspended in media via agitation and provide the available surface area for hMSC expansion [4, 13]. A variety of microcarriers are commercially available depending on the intended applications, which generally range from 100 to 300 μm in diameter and are synthesized with materials such as polystyrene, dextran, polyvinyl alcohol, glass, etc. [14-16]. Additional protein coatings can be applied to microcarriers to facilitate cell adhesion such as collagen, cellulose, fibronectin, etc. Microcarriers also can be fabricated using porous materials to increase surface area for cell growth, however, this may reduce the efficiency of downstream hMSC harvesting.

Suspension bioreactor microenvironment differs from static planar culture in dynamic forces encountered. Constant agitation from the impeller induces fluid flow and shear stress. Depending on the type of microcarriers, and the geometry of the vessels and impellers, varying agitation rates have been used in numerous studies [13, 17, 18]. However, it is common practice to use the lowest agitation speed necessary to suspend microcarriers in media in order not to alter gene expression or damage cells. Ismadi et. al., implemented Particle Image Velocimetry to quantify velocity and shear stress encountered at varying positions within the spinner flask bioreactor [19]. The authors found fluid velocity and shear stress vary throughout the reactor with high velocities measured at the tip of the impeller near the flask sidewall as well as near the bottom of the flask. Similarly, the location of the highest shear stress was close to the bottom of the flask. When the agitation speed was increased from 10 rpm to 80 rpm, the average velocity, average shear stress, the maximum velocity and maximum shear stress increased linearly.

Since hMSC phenotype is sensitive to changes in microenvironment, previous studies investigating and optimizing hMSC therapeutic potency in static planar cultures may differ from suspension bioreactors as certain hMSC characteristics are known to be altered under shear stress. For example, shear stress has been shown to enhance osteogenic differentiation [20]. Similarly, the upregulation of chondrogenic genes in cultures exposed to shear stress was observed as well as increased extracellular matrix (ECM) deposition and collagen type II secretion [21]. In addition to differentiation, shear stress also affects immunomodulatory abilities of hMSCs [22]. Diaz et. al. showed that subjecting hMSCs to fluid flow increased the secretion of prostaglandin E2 (PGE2) as well as the potential to suppress tumor necrosis factor (TNF)-α production. This discrepancy between static planar culture and spinner flask bioreactor culture, although still not entirely understood, has gained recognition [4]. Despite that agitation can fundamentally alter underlying metabolic processes, little investigation of shear stress on the cellular aging process has been reported [23]. Therefore, this study sought to test the hypothesis that shear stress modulates human MSC homeostasis which may affect therapeutic properties, while still maintaining growth kinetics within the microcarrier-based suspension bioreactor. The long-term goal of this study is to yield larger numbers of therapeutically potent hMSCs.

2. Materials and Methods

2.1. hMSC Static Planar Culture

Frozen hASCs at passage 1 were acquired from Tulane Center for Stem Cell Research and Regenerative Medicine. The human adipose-derived MSCs (hASCs) were isolated from the subcutaneous abdominal adipose tissue from de-identified healthy donors. Similarly, bone marrow-derived MSCs (BM-MSC) were isolated from human bone marrow of de-identified healthy donors at Tulane Center. The isolated human MSCs were characterized for colony-forming unit (CFU) as well as tri-lineage differentiation potential (osteogenic, adipogenic and chondrogenic differentiation) *in vitro*. The received hMSCs (1×10^6 cells/ml/vial) frozen in minimum essential medium-alpha (α-MEM) supplemented with 2 mM L-glutamine, 30% fetal bovine serum (FBS), and 5% dimethyl sulfoxide were thawed and cultured as described in our previous publications [24, 25]. Briefly, hMSCs were seeded at a density of 1,500 cells/cm^2 in 150 mm diameter Petri Dishes (Corning, Corning, NY) in a standard 5% CO_2 incubator. Cells were cultured in α-MEM (Life Technologies, Carlsbad, CA) with 10% FBS (Atlanta Biologicals, Lawrenceville, GA) and 1% Penicillin/Streptomycin (Life Technologies) and media were changed every 2-3 days. Cells were grown to 80% confluence and then harvested by incubation with 0.25% trypsin/ethylenediaminetetraacetic acid (EDTA) (Invitrogen, Grand Island, NY) for no greater than 7 minutes. Enzymatic digestion was stopped using 8 mL of fresh media. The solution was pelleted via centrifugation (500 g) for 5 min. Cell pellet was resuspended in 1 mL of fresh media and sampled for cell count and viability. Harvested cells were sub-cultured up to passage 6 before seeding in the spinner flask bioreactors.

2.2. hMSC Expansion in Spinner Flask Bioreactors

Plastic Plus Microcarriers (PP; 0.7 g, SoloHill, Ann Arbor, MI) were hydrated overnight in phosphate-buffered saline (PBS). 1 gram of PP is approximately equal to 360 cm^2 of cell culture surface area. PP were then washed three times with 10 mL of fresh PBS and resuspended in 30 mL of fresh PBS. Mixture was autoclaved to sterilize microcarriers and PBS is aspirated and replaced with fresh serum containing media. PP were washed two more times with fresh media ensuring complete removal of PBS and then allowed to incubate in the media for greater than two hours to facilitate adhesion of attachment proteins in the serum to the microcarriers.

Half the working volume, 30 mL, was used for seeding to enhance cell attachment efficiency by increasing cell and microcarrier interactions within the 125 mL Wheaton Celstir®Suspension Culture spinner flask (VWR international, Rad-nor, PA) with Wheaton Biostir® Stirrers system (**Figure 1**) [13, 26]. Cells were inoculated at a concentration of 4.2×10^4 cells/mL seeding volume for a total of 1.25×10^6 cells/flask. The seeding phase consisted of 32 cycles each lasting 20 minutes. One cycle was complete after 4 minutes of agitation (50 rpm) followed by 16 minutes of no agitation. 50 rpm is the minimum agitation speed in this geometry with PP required to have complete suspension of microcarriers. After the seeding, 50% of the media was changed to remove any unattached cells and 60 mL working volume was agitated at 50 rpm during culture.

A feeding schedule consisted of a 50% media change every 2 days. Samples were taken at 1 mL on day 1, 3, and 5 to check growth kinetics, and visually inspect the cells. The spent media samples were taken for glucose and lactate analysis. Cell number was determined by Quant-iT™ PicoGreen kit (Invitrogen, Grand Island, NY). To visually inspect cell attachment, cells on microcarriers were stained with Hoechst 33342 (Thermofisher) to reveal cell nuclei and imaged under an Olympus IX70 microscope. After 7 days, cells were harvested for various assays.

2.3. Cell Number Determination

Cell number was determined by Quant-iT™ PicoGreen kit (Invitrogen, Grand Island, NY), following the methods reported previously [25]. Briefly, cells were harvested, lysed over-night using proteinase K (VWR, Radnor, PA), and stained with Picogreen (Molecular Probes, Eugene, OR) to allow quantitation of cellular DNA using a standard curve. Fluorescence signals were read using a Fluror Count (PerkinElmer, Boston, MA). Cell number was calculated from the amount of DNA detected.

2.4. Biochemical Assays

MTT assay: The cell samples were incubated with 5 mg/mL MTT (Sigma) solution. Then a 10X dilution was used per well as a final concentration. The MTT solution was incubated for an hour at 37ºC. Then, the media and MTT were removed and the formazan crystals were dissolved in DMSO, centrifuged at 800 g for 5 minutes. Then the absorbance of the supernatants was measured at 490 nm on a plate reader (BioRad).

Glucose/Lactate concentrations: Fresh and spent media were collected to determine glucose consumption and lactate production by YSI 2500 Biochemistry Select Analyzer (Yellow Spring, OH). Cellular DNA damage was measured by comet assay (Cell Biolabs, Inc. San Diego, CA), following manufacturer's instructions.

Reactive oxygen species (ROS) assay: For ROS measurement, cell suspension was incubated with 25 µM carboxy-H2DCFDA (Molecular Probe) at 37°C for 30 min and total ROS was determined using flow cytometry. For mitochondrial ROS measurement, cell suspension was incubated with 5 µM MitoSOX Red (Molecular Probe) at 37°C for 10 min and analyzed using flow cytometry.

2.5. Measurement of Indoleamine 2,3-dioxygenase (IDO) Activity

For IDO enzymatic activity, including both IDO1 and IDO2 (both convert Tryptophan to Kynurenine) was assessed by measuring Kynurenine level in cell culture supernatant. A 400 µl supernatant from hMSCs culture, either stimulated by interferon (IFN) γ at 40 ng/mL or left unstimulated for 24 hours until sample collection, was clarified by mixing with trichloroacetic acid (200 µl, 30% by weight; Sigma Aldrich, St. Louis, MO) by vortex, followed by centrifugation at 8,000xg for 5 minutes. An equal volume of Ehrlich reagent (2% p-dimethylaminobenzaldehyde in glacial acetic acid) was added to the clarified supernatant, and optical density at 490 nm was measured.

2.6. Immunocytochemistry and Flow Cytometry

Cells were harvested from monolayer culture or microcarrier bioreactors by incubation with 0.25% trypsin–EDTA solution for 5–7 minutes at 37°C. Suspended hMSCs were washed in PBS, and fixed at 4% paraformaldehyde (PFA) at room temperature for 15 minutes. Cells were then permeabilized in 0.2% triton X-100 PBS for 10 minutes at room temperature (RT). Nonspecific binding sites were blocked in PBS with 1% bovine serum albumin, 10% goat serum, 4% nonfat dry milk for 15 minutes at room temperature (RT). After washing with PBS, cells were incubated with primary antibodies at RT for two hours, followed by one hour incubation with FITC conjugated secondary antibody (Molecular Probe, Eugene, OR) at RT. Labeled samples were washed in PBS and acquired using BD FACSCanto II flow cytometer (Becton Dickinson) along with isotype control. The results were analyzed using FlowJo software.

2.7. Enzyme-linked Immunosorbent Assay (ELISA) for PGE2 Secretion

Secreted PGE2 in cell culture supernatants was quantified using a PGE2 Parameter Assay Kit (R&D Systems, Minneapolis, MN) according to manufacturer's instructions. Total secreted PGE2 was determined by subtracting cytokine concentrations in culture media controls and normalized to cell number.

2.8. Intracellular NAD^+ and NADH Quantification

Intracellular NAD^+ and NADH were measured with NAD^+/NADH Quantification Colorimetric Kit (BioVision, Milpitas, CA) according to manufacturer's instructions with some modifications. Briefly, approximate 0.8 million cells were collected and directly lysed in 200 µL lysis buffer from the assay kit. The volume of reagents in each step was scaling down by 50% and the results were calculated by the freshly prepared standard curve (NADH standards provided by the assay kit). Final NAD^+ and NADH concentrations were then normalized to the total cell number in each group.

2.9. Western Blot

Human MSCs were washed with PBS, and lysed in radio-immunoprecipitation assay (RIPA) buffer (150 mM sodium chloride, 1.0% Trition X-100, 0.5% sodium deoxycholate, 0.1% sodium dodecyl sulfate, 50 mM Tris, pH 8, 2 µg/mL Aprotinin, 5 µg/mL Leupeptin, 5 µg/mL Antipain, 1 mM PMSF protease inhibitor), and homogenized by sonification using a Sonic Dismembrator 100 (Fisher Scientific, Hampton, NJ). Samples were then digested for 20 min on ice, and spun down at 14,000 rpm for 20 min. The supernatant was collected and a Bradford assay was carried out to determine the protein concentration. The samples were denatured at 95°C in 2 x Laemmli Sample buffer. Proteins were separated by 15% BIS-Tris-SDS gels and transferred onto a nitrocellulose membrane (Bio-rad, Hercules, CA). For the detection of non-phosphorylated proteins, the membranes were blocked for 30 min in 3% skim milk (w/v) in Tris-buffered saline (10 mM Tris-HCl, pH 7.5, and 150 mM NaCl) with 0.1% Tween 20 (v/v) (TBST), or in 3% bovine serum albumin in TBST. Membranes were incubated overnight in the presence of the primary Sirt-1, Sirt-3, and α-tubulin antibody diluted in the corresponding blocking buffer at 4°C. Afterward, the membranes were washed four times for 10 min each with TBST and then incubated with an IR

secondary (LI-COR, Lincoln, NE) at 1:10,000 for 180 min at room temperature. Blots were washed another four times for 10 min each with TBST and processed using the LI-COR Odyssey.

2.10. Statistical Analysis

Unless otherwise noted, all experiments were performed at least in triplicate (n=3), and representative data are reported. Experimental results are expressed as means ± standard deviation (SD) of the samples. Statistical comparisons were performed by one-way ANOVA and Tukey's post hoc test for multiple comparisons, and significance was accepted at $p < 0.05$.

3. Results

3.1. Physiology of BM-MSCs and optimization of microcarrier cultures.

The human BM-MSCs are usually expanded on tissue culture surface with normal spindle shape, expressing E-cadherin (**Supplementary Figure S1A**). They can also form hMSC aggregates, also referred as mesenchymal bodies [27] **(Supplementary Figure S1B**). The size of hMSC aggregates can be controlled by the seeding cell number and upon replating, the hMSC aggregates show the single cell outgrowth and migration ability **(Supplementary Figure S1C**). β-gal staining shows the cellular senescence in both replated hMSC aggregates and 2D expanded hMSCs (**Supplementary Figure S1D**). The hMSCs exhibit immunomodulatory ability for both 2D cells and hMSC aggregates, indicated by IDO activity induced by IFNγ **(Supplementary Figure S2A**). Increased aggregation decreased hMSC IDO activity. hMSC IDO response did not show concertation-dependence when IFNγ concentration passes 5 ng/mL (**Supplementary Figure S2B**). In 2D cultures, IFNγ treatment increased cell response, while increasing seeding density decreased IDO response (**Supplementary Figure S2C**).

To adapt BM-MSCs to microcarrier culture in suspension spinner bioreactor, four different microcarrier types (i.e., Cydodex I, Helix, Plastic, and Plastic plus) were tested for hMSC attachment in static culture (**Supplementary Figure S3A**). Plastic type microcarriers were coated with FBS or collagen to improve hMSC attachment. FBS coating appeared to improve overall cell attachment compared to collagen (**Supplementary Figure S3B**). Hoechst-staining of the microcarriers with cells showed adequate attachment of hMSCs for both Cytodex I and Plastic plus microcarriers (**Supplementary Figure S3C).** hMSCs on collagen and FBS-coated plastic

microcarriers showed a similar capacity to be dissociated from microcarriers and replated as static planar cultures (**Supplementary Figure S4A**). After dissociation from microcarriers, hMSCs showed ability to proliferate and maintain spindle shape compared to 2D hMSC culture (**Supplementary Figure S4B**). Based on these results, Plastic plus microcarriers with FBS coating was used for the following experiments unless otherwise noted.

3.2. Effects of agitation on BM-MSC expansion in microcarrier-based spinner bioreactors.

To observe the effects of agitation on hMSCs in microcarrier-based bioreactor systems, hMSCs were grown at 50 and 70 rpm. Hoechst-staining images show the ability of hMSCs to attach and expand in the culture under different agitation rates **(Figure 2A)**. DNA assay indicates that hMSCs expand in spinner flasks at 50 rpm (1.5-1.6 fold during day 1-7), while for 70 rpm, cells did not show expansion **(Figure 2B)**. Variations were observed between the duplicate bioreactors. As expected, during cell proliferation in the bioreactor (50 rpm), glucose levels decreased while lactate levels increased (**Figure 2C**). The ratio of lactate production to glucose consumption (g/g) increased from 0.5 at day 1-2 to 1.0 at day 6-7 (**Figure 2D**), showing that high cell density during day 6-7 may result in anaerobic metabolism. To validate the results, the hMSCs were expanded in microcarrier-based bioreactor systems at 50 rpm and 70 rpm in another run. For 50 rpm, bioreactor 2 showed 1.5-fold expansion during day 1-7, while bioreactor 1 showed less expansion (**Figure 3**). For 70 rpm, Hoechst-staining images indicate the ability of hMSCs to expand in this run (**Figure 4A**). In particular, bioreactor 2 showed 3-fold expansion during day 1-7, while bioreactor 1 showed 2.5-fold expansion indicated by MTT assay and DNA assay (**Figure 4B and 4C**). The variations among different bioreactor runs may be attributed to the quality of initial seeded BM-MSCs. Taken together, the hMSCs can be expanded in microcarrier-based bioreactor systems during 50-70 rpm.

BM-MSCs expansion on Cytodex I microcarriers in spinner bioreactors was also evaluated at 30 rpm and 85 rpm (**Supplementary Figure S5**). Compared with 85 rpm, the 30 rpm agitation was observed to support higher MTT metabolic activity and glucose consumption, which is usually associated with higher cell growth rate (**Supplementary Figure S5A, S5B, S5C**). In particular, cells harvested from 30 rpm and 85 rpm bioreactors as well as 2D culture were evaluated by flow cytometry for cell size distribution, indicated by forward scatter histogram (**Supplementary**

Figure S5D). Cells from bioreactors (both at 30 rpm and 85 rpm) showed much smaller cell size compared to cells from 2D culture.

To determine whether hMSC passage number affects cell growth, P4 and P6 hMSCs were cultured in the microcarrier-based spinner flask bioreactors. Regardless of passage number, Hoechst staining images show that hMSCs attached onto microcarriers **(Supplementary Figure S6A)**. The DNA assay showed no significant difference between the P4 or P6 hMSCs in bioreactor culture **(Supplementary Figure S6B).** The feeding schedule was varied as seen in some experiments (**Supplementary Figure S7**), and the alternate half medium change was used in bioreactor culture unless otherwise noted.

To determine the effect of agitation on immune response of hMSCs, bioreactor-derived hMSCs and 2D-grown hMSCs were treated with IFNγ. The IDO response was greater for bioreactor-derived cells in both the IFNγ-treated and untreated groups (**Figure 5A**). The response to IFNγ treatment also appears to diminish after bioreactor-derived hMSCS were allowed to reattach on tissue culture surface for two days (**Figure 5B**).

3.3. hASC expansion in microcarrier-based spinner bioreactors.

Following the similar seeding method for BM-MSCs, roughly 80% of hASCs attach to microcarriers (data not shown) with a near homogeneous distribution of cells onto microcarriers (**Figure 6A).** hASC proliferation in the spinner flask bioreactor first underwent a lagging phase (1-3 days) followed by exponential growth, especially when the cells were seeded at a lower density (0.7×10^6 cells at day 1 which grew to 1.25×10^6 cells at day 7) (**Figure 6B)**. In the runs with a high seeding density (1.5×10^6 cells at day 1), the lag phase was short and the growth curve reached plateau after day 5 (3.6×10^6 cells at day 5) (**Figure 6C and 6D**). This may occur because the confluence is reached on majority of microcarriers. Total cell numbers increased 2.4-3.2 fold over the course of the 7 days of culture. However, metabolic activity as measured by MTT assay showed the plateau or decrease after day 3, suggesting that the metabolic activity per cell decreased with the expansion and the physiological change occurs during the expansion.

3.4. Effects of microcarrier-based spinner bioreactor culture on NAD+/NADH ratio and Sirt1/Sirt3 expression in hASCs.

Since hMSC functionality is sensitive to shear stress and other environmental factors [28], the underlying metabolism and immune-modulation capability of hMSCs grown in the spinner

flask relative to static planar culture were investigated. Since the downstream functions depend on NAD-consuming mediators, the cytoplasmic and mitochondrial NAD+/NADH ratio should be maintained [29]. Our results found that the cells from the microcarrier-based spinner flask had similar NAD+/NADH ratio compared to static planar culture (**Figure 7A**). Similarly, similar expression of NAD-dependent Sirt1 was observed (**Figure 7B(i)**). However, Sirt3 expression was higher for the cells from the microcarrier-based spinner flask compared to static planar culture (**Figure 7B(ii)**). The increased Sirt3 expression in the cells from spinner flasks most likely is attributed to the increased ROS, as Sirt3 is known to play a role in ameliorating oxidative stress [30]. Western blot analysis also showed similar Sirt1 expression and higher Sirt3 for microcarrier-based spinner flask compared to static planar culture (**Figure 7C**). However, the *in vitro* expanded cells in planar culture to a high passage (passage 12) showed the decrease in Sirt1 expression compared to low passage cells (passage 5), indicating the age-related senescence [31].

3.5. Effects of agitation on PGE2 secretion and IFNγ-induced immune response in hASCs.

Knowing that shear stress activates specific signaling in hMSCs to regulate immune cells (e.g., HMOX1, PTGS2) [22], it is hypothesized that the key secreted immunoregulatory factors would be altered by exposure to shear stress in the spinner flask bioreactors. Over the first 24 hours of culture, hMSCs secreted over 50-fold higher PGE2 (normalized to cell number) compared to static planar culture (**Figure 8A**). Similarly, basal and IFNγ-treated IDO activity of hMSCs measured through kynurenine concentrations showed the increased activity compared to static planar culture (**Figure 8B**), suggesting the increased immunosuppressive ability.

In order to illustrate the differences between microcarrier-based spinner flask bioreactors and the static 2D culture, total ROS was quantified using flow cytometry. The mean fluorescence intensity of ROS increased in spinner flask cultures compared to static planar cultures, due to increased cellular stress from dynamic microenvironment (**Figure 8C**). Aside from the metabolic differences, spinner flask-cultured cells had smaller size compared to 2D culture as shown by forward scatter intensity through flow cytometry (**Figure 8D**), which was consistent with the results of Supplementary Figure S5D.

4. Discussion

Previous decade has seen significant advances in hMSC applications in preclinical and clinical trials as a treatment for myocardial infraction, spinal cord injury, immunological diseases, etc. [32, 33]. However, systems must be engineered and adapted from traditional planar cultures to yield practical numbers of therapeutically potent cells. Microcarrier-based suspension bioreactors are an attractive approach that can offer high cell yields per unit volume and the control over microenvironment [4].

4.1. Microcarrier-based MSC expansion in suspension bioreactors.

Choice of microcarriers can have a significant impact on culture conditions and expansion. In this study, plastic plus microcarriers were chosen for achieving seeding efficiency of 70%-80% (data not shown), potential for modest expansion folds (with surface area of 360 cm^2/g), and their compatibility with enzymatic treatment for hMSC harvesting. Although other types of microcarriers, such as Cytodex I (4400 cm^2/g), have achieved greater seeding efficiency and hMSC expansion than plastic plus microcarriers [18, 34], it has been noted that enzymatic cell harvesting is inefficient [35]. Therefore, Cytodex I microcarriers may be better suited for applications where hMSCs are not the direct products, for example the production of exosomes where high cell density could provide concentrated conditioned media. Other parameters affected by the type of microcarriers include the extent of cell clumping and the use of xeno-free medium [11, 36].

As it has been suggested, underlying energy metabolism has a profound effect on hMSC functionality [37]. Metabolite monitoring can be a notable metric for estimating energy production efficiency under different conditions. During anaerobic glycolysis, glucose catabolism yields 2 mol of ATP and 2 mol of lactate per mol of glucose consumed [38]. Therefore, an observed mole ratio of lactate production to glucose consumption of 2 could indicate the primary energy source based on glycolysis. Furthermore, it has been shown that hMSC proliferation can be hindered by excess levels of lactate (35.4 mM) and ammonia (2.4 mM) [39]. An optimized feeding strategy mainly focuses on preventing glucose depletion and avoiding exceeding levels of lactate and ammonia concentrations that can be potentially detrimental to proliferation. Our study empirically found a 50% media change maintained metabolite concentrations and promoted hMSC proliferation, which are consistent with other studies [17, 18]. The possible effect of other

parameters such as nutrients, cell density, and gas sparging can be found in our previous publication [4].

The shear stress profiles in our spinner flask bioreactor (30-70 rpm) were simulated using COMSOL software (**Supplementary Figure S8, S9, S10, and S11**). It was found that shear stress was not homogenous throughout the bioreactor (e.g., there is a low shear stress zone under the impeller) and varied with respect to position (1-9 dyn/cm^2). Our simulated shear stress spikes around the edges of the impeller consistent with other studies [19, 40]. Similarly, increasing impeller rotation speed corresponds to a linear increase in average shear stress (2-5 dyn/cm^2) encountered in the spinner flask by the hMSCs. Heathman et. al., demonstrated that increasing impeller speed from 80 rpm to 225 rpm had a significant impact on cell proliferation [23]. Our study showed increasing the impeller speed of 50 rpm was not significant enough to curtail proliferation, but can enhance the immunomodulatory ability of the hMSCs.

4.2. The effects of shear stress on hMSC immunomodulatory ability.

Following stimulation with IFNγ, hMSCs exhibit immunosuppressant effect on surrounding immune cells through cell-cell contact and secretion of soluble factors such as IL-10, TGF-β, NO, IDO, TSG6, and PGE2 [41]. These factors can affect the adaptive immune system (inhibiting T cell and B cell proliferation) and the innate immune system, inhibiting activation of dendritic cells (DCs) and proliferation of natural killer (NK) cells [42].When sub-optimally activated (via IFNγ), MSCs secrete chemokines but do not produce adequate concentrations of IDO to suppress T cells, B cells, DCs, and NK cells [41]. IDO is involved in the catabolism of tryptophan into kynurenines mediating the kynurenine pathway [43]. The kynurenine pathway depletes tryptophan, ultimately suppressing the mammalian target of rapamycin (mTOR) pathway and inhibiting Teff cell function, as well as promotes CD4+ T cell differentiation into Treg cells and inhibits IL-2 signaling to reduce memory CD4+ T cell survival [43]. In this study, our results show that shear stress encountered in the spinner flask enhances IDO activity and PGE2 secretion of hASCs compared to static planar culture. Further functional assays need to be conducted to determine if this augmented IDO production translates into strengthened hMSC immunosuppressive abilities of the adaptive and innate immune system.

Biophysical cues have a direct impact on biochemical signaling within hMSCs, which causes cytoskeletal rearrangement and alters lineage specification [44, 45]. The wall shear stress

was reported to promote PGE2 secretion through NFκB-COX2-PGE2 signaling axis to suppress TNF-α for bone marrow MSCs [22]. After subjecting hMSCs to 15 dyne/cm^2 for short time intervals, COX2 and Heme oxygenase-1 (an anti-inflammatory enzyme) were significantly upregulated. hMSCs exposed to shear stress also displayed enhanced immunosuppressive function that suppresses TNF-α production. Overexpression of COX2 has been shown to enhance the immunosuppressive function of hMSCs [46]. Shear stress was also shown to upregulate genes responsible for anti-inflammatory function (e.g., *PTGS2, HMOX1, IL1RN,* and *TNFAIP6*) and stimulate the Akt, the mitogen-activated protein kinase (MAPK), and focal adhesion kinase (FAK) signaling pathways [47]. FAK signaling through wall shear stress regulation of bone marrow MSCs also stimulates COX2 induction to promote anti-inflammatory activity and suppress TNF-α production by activated immune cells [47].

4.3. NAD+/NADH redox and Sirt1/Sirt3 in hMSCs from microcarrier-based bioreactors.

Stem cells are known to exhibit metabolic plasticity in order to meet energy demands for self-renewal and lineage specification. Low passage hMSCs are generally a clonogenic subset expressing high glycolytic activity. *In vitro* passaging has been shown to increase ROS accumulation [48] and cause an imbalance to the NAD+/NADH redox cycle, leading to mitochondrial damage and cellular senescence [49, 50] and a loss of cellular homeostasis and functional decline [31]. This is in part due to the non-redox roles of NAD+ as a substrate for ADP-ribosyltransferase (ARTDs) and Sirtuin enzymes that mediate essential functions vital to cell longevity. The Sirtuin family is a 7-enzyme family linked to genome stability, mitochondrial and oxidative metabolism, and lifespan regulation [51]. Specifically, Sirt1 and Sirt3 are of interest due to their high Michaelis constants (94-96 and 880 μM respectively), allowing them to serve as indicators of NAD+ levels [52].

Our results found that in short term culture (one week) NAD+/NADH ratios were similar between static planar-cultured and spinner flask-cultured hMSCs. Sirt1 expression remains unchanged but Sirt3 expression increased by exposing to shear stress. Total ROS increase and smaller cell size most likely accounted for the increase in NAD+-dependent Sirt3 expression in an attempt to ameliorate oxidative stress [30]. In fact, reduced cell size is desired for administration of hMSCs in ischemic stroke treatment to reduce the risk of random embolism or lacunar stroke [53]. Increase of ROS and metabolic reconfiguration towards oxidative phosphorylation indicate

potential senescence of hMSCs during culture expansion and have significantly compromised the therapeutic efficacy of hMSCs [31]. However, this study only observed ROS increase, not the alterations of NAD+/NADH redox cycle in the cells form bioreactors. These results suggest the stress in bioreactor may be different compared to extensive culture induced senescence and may have limited effects on the hMSC efficacy. Since increased ROS is associated with oxidative stress and DNA damage, increased expression of ARTDs would be expected, which may lead to ARTD-mediated cell death [51]. Interestingly, ROS production can be attributed to aerobic respiration as well as by COX-2 during arachidonic acid metabolism into PGE2. Therefore, further investigations should take place into if the increase in ROS is due to shifts in energy metabolism or immune response.

In addition, it has been suggested that the maintenance of high glycolytic activity is cytoprotective for cells, as some byproducts of the pentose phosphate pathway are anti-oxidant precursors [37]. Similarly, nutrient-responsive metabolites have been shown to mediate crosstalk between metabolism and cellular signaling [54], suggesting that metabolism and cell fate are intertwined. In fact, there is ample evidence linking metabolism in hMSCs to proliferation potential [55], stemness and differentiation [56], and immune response [25]. Liu et. al. found that IFNγ activation of Akt/ mTOR signaling is required for metabolic remodeling and for IDO and PGE2 production in hMSCs, which is sustained by glycolysis. Furthermore, treatments reducing oxidative phosphorylation activity further enhanced IDO production. What has yet to be seen is if the shear stress activation of the hMSC immunomodulatory repertoire undergoes the similar metabolic reprogramming process as IFNγ licenses hMSCs towards a more glycolytic dependent subset. Then by extension, if this enhanced glycolytic activity still acts in a cytoprotective manner for the hMSCs to preserve the NAD+/NADH balance and prevent functional decline.

5. Conclusion

This study demonstrates hMSC expansion of 3-fold over seven days in microcarrier-based spinner flask bioreactors. Furthermore, our results indicate a fundamental shift in underlying hMSC properties from static planar culture to spinner flask bioreactor culture leading to an enhanced immunosuppressive phenotype and PGE2 secretion. Although short-term culture does not alter NAD+/NADH ratios and Sirt1 expression, the increased ROS production, Sirt3 expression, and smaller cell size could have implications on cellular homeostasis. In particular,

this study implements an engineering strategy to enhance hMSC immune-regulatory abilities. The results of this study provides insight for scalable production of hMSCs utilized in biomanufacturing and clinical trials.

6. Acknowledgement

In fond memory, the authors acknowledge guidance provided by Professor Teng Ma for the worked performed by S.L. The authors would like to thank Ms. Ruth Didier in FSU Department of Biomedical Sciences for her help with flow cytometry analysis, Dr. Bruce Bunnell at Tulane Center for hMSCs, and Dr. Samuel Grant for helping S.L. This work is partially supported by National Science Foundation (CBET-No. 1743426 and 1917618). Research reported in this publication was also supported by the National Institutes of Health (USA) under Award Number R01NS102395. The content is solely the responsibility of the authors and does not necessarily represent the official views of the National Institutes of Health.

7. Declarations

The authors declare that they have no competing interests.

References:

[1] J.M. Gimble, F. Guilak, M.E. Nuttall, S. Sathishkumar, M. Vidal, B.A. Bunnell, In vitro Differentiation Potential of Mesenchymal Stem Cells, Transfus Med Hemother, 35 (2008) 228-238.

[2] C.W. Park, K.-S. Kim, S. Bae, H.K. Son, P.-K. Myung, H.J. Hong, H. Kim, Cytokine secretion profiling of human mesenchymal stem cells by antibody array, Int J Stem Cells, 2 (2009) 59-68.

[3] J.M. Ryan, F.P. Barry, J.M. Murphy, B.P. Mahon, Mesenchymal stem cells avoid allogeneic rejection, J Inflamm (Lond), 2 (2005) 8.

[4] A.C. Tsai, R. Jeske, X. Chen, X. Yuan, Y. Li, Influence of microenvironment on mesenchymal stem cell therapeutic potency: from planar culture to microcarriers, Front Bioeng Biotechnol, 8 (2020) 640.

[5] B.M. Bijonowski, Q. Fu, X. Yuan, J. Irianto, Y. Li, S.C. Grant, T. Ma, Aggregation-induced Integrated Stress Response Rejuvenates Stemness of Culture-Expanded Human Mesenchymal Stem Cells., Biotechnol Bioeng, 117 (2020) 3136-3149.

[6] B.M. Bijonowski, X. Yuan, R. Jeske, Y. Li, S.C. Grant, Cycling aggregation extends in vitro expansion potential of human mesenchymal stem cells, Sci Rep, 10 (2020) 20448.

[7] R. Jeske, X. Yuan, Q. Fu, B. Bunnell, T.M. Logan, Y. Li, In Vitro Culture Expansion Shifts the Immune Phenotype of Human Adipose-derived Mesenchymal Stem Cells., Front Immunol, In Press (2021).

[8] M. Kabat, I. Bobkov, S. Kumar, M. Grumet, Trends in mesenchymal stem cell clinical trials 2004-2018: Is efficacy optimal in a narrow dose range?, STEM CELLS Translational Medicine, 9 (2020) 17-27.

[9] T. Lawson, D.E. Kehoe, A.C. Schnitzler, P.J. Rapiejko, K.A. Der, K. Philbrick, S. Punreddy, S. Rigby, R. Smith, Q. Feng, J.R. Murrell, M.S. Rook, Process development for expansion of human mesenchymal stromal cells in a 50L single-use stirred tank bioreactor, Biochem Eng J, 120 (2017) 49-62.

[10] G. Eibes, F. dos Santos, P.Z. Andrade, J.S. Boura, M.M.A. Abecasis, C.L. da Silva, J.M.S. Cabral, Maximizing the ex vivo expansion of human mesenchymal stem cells using a microcarrier-based stirred culture system, J Biotechnol, 146 (2010) 194-197.

[11] F. Dos Santos, A. Campbell A Fau - Fernandes-Platzgummer, P.Z. Fernandes-Platzgummer A Fau - Andrade, J.M. Andrade Pz Fau - Gimble, Y. Gimble Jm Fau - Wen, S. Wen Y Fau - Boucher, M.C. Boucher S Fau - Vemuri, C.L. Vemuri Mc Fau - da Silva, J.M.S. da Silva Cl Fau - Cabral, J.M. Cabral, A xenogeneic-free bioreactor system for the clinical-scale expansion of human mesenchymal stem/stromal cells. Biotechnol Bioeng, 111 (2014) 1116-1127.

[12] S. Sart, S.N. Agathos, Y. Li, T. Ma, Regulation of mesenchymal stem cell 3D microenvironment: From macro to microfluidic bioreactors, Biotechnol J, 11 (2016) 43-57.

[13] A.C. Tsai, T. Ma, Expansion of Human Mesenchymal Stem Cells in a Microcarrier Bioreactor, Methods Mol Biol, 1502 (2016) 77-86.

[14] Q.A. Rafiq, K. Coopman, A.W. Nienow, C.J. Hewitt, Systematic microcarrier screening and agitated culture conditions improves human mesenchymal stem cell yield in bioreactors, Biotechnol J, 11 (2016) 473-486.

[15] M.J. Varani J Fau - Bendelow, J.H. Bendelow Mj Fau - Chun, W.A. Chun Jh Fau - Hillegas, W.A. Hillegas, Cell growth on microcarriers: comparison of proliferation on and recovery from various substrates. J Biol Stand, 14 (1986) 331-336.

[16] S. Sart, S.N. Agathos, Y. Li, Engineering stem cell fate with biochemical and biomechanical properties of microcarriers, Biotechnol Prog, 29 (2013) 1354-1366.

[17] R. Das, R. Roosloot, M. van Pel, K. Schepers, M. Driessen, W.E. Fibbe, J.D. de Bruijn, H. Roelofs, Preparing for cell culture scale-out: establishing parity of bioreactor- and flask-expanded mesenchymal stromal cell cultures, J Transl Med, 17 (2019) 241.

[18] D. Schop, R. van Dijkhuizen-Radersma, E. Borgart, F.W. Janssen, H. Rozemuller, H.J. Prins, J.D. de Bruijn, Expansion of human mesenchymal stromal cells on microcarriers: growth and metabolism, J Tissue Eng Regen Med, 4 (2010) 131-140.

[19] K.H. Mohd-Zulhilmi Ismadi, Andreas Fouras, Experimental Characterisation of Fluid Mechanics in a Spinner Flask Bioreactor, Processes, 2 (2014) 753-772.

[20] G. Yourek, S.M. McCormick, J.J. Mao, G.C. Reilly, Shear stress induces osteogenic differentiation of human mesenchymal stem cells, Regen Med, 5 (2010) 713-724.

[21] M.L. Alves da Silva, A.R. Martins A Fau - Costa-Pinto, V.M. Costa-Pinto Ar Fau - Correlo, P. Correlo Vm Fau - Sol, M. Sol P Fau - Bhattacharya, S. Bhattacharya M Fau - Faria, R.L. Faria S Fau - Reis, N.M. Reis Rl Fau - Neves, N.M. Neves, Chondrogenic differentiation of human bone marrow mesenchymal stem cells in chitosan-based scaffolds using a flow-perfusion bioreactor. J Tissue Eng Regen Med, 5 (2011) 722-732.

[22] M.F. Diaz, A.B. Vaidya, S.M. Evans, H.J. Lee, B.M. Aertker, A.J. Alexander, K.M. Price, J.A. Ozuna, G.P. Liao, K.R. Aroom, H. Xue, L. Gu, R. Omichi, S. Bedi, S.D. Olson, C.S. Cox, Jr., P.L. Wenzel, Biomechanical Forces Promote Immune Regulatory Function of Bone Marrow Mesenchymal Stromal Cells, Stem Cells, 35 (2017) 1259-1272.

[23] T.R.J. Heathman, A.W. Nienow, Q.A. Rafiq, K. Coopman, B. Kara, C.J. Hewitt, Agitation and aeration of stirred-bioreactors for the microcarrier culture of human mesenchymal stem cells and potential implications for large-scale bioprocess development, Biochem Eng J, 136 (2018) 9-17.

[24] L. Song, X. Yuan, Z. Jones, K. Griffin, Y. Zhou, T. Ma, Y. Li, Assembly of human stem cell-derived cortical spheroids and vascular spheroids to model 3-D brain-like tissues, Sci Rep, 9 (2019) 5977.

[25] Y. Liu, X. Yuan, N. Munoz, T.M. Logan, T. Ma, Commitment to Aerobic Glycolysis Sustains Immunosuppression of Human Mesenchymal Stem Cells, Stem Cells Transl Med, 8 (2019) 93-106.

[26] X. Yuan, A.C. Tsai, I. Farrance, J. Rowley, T. Ma, Aggregation of Culture Expanded Human Mesenchymal Stem Cells in Microcarrier-based Bioreactor, Biochem Eng J, 131 (2018) 39-46.

[27] S. Sart, R.F. Tomasi, A. Barizien, G. Amselem, A. Cumano, C.N. Baroud, Mapping the structure and biological functions within mesenchymal bodies using microfluidics, Sci Adv, 6 (2020) eaaw7853.

[28] P. Becquart, M. Cruel, T. Hoc, L. Sudre, K. Pernelle, R. Bizios, D. Logeart-Avramoglou, H. Petite, M. Bensidhoum, Human mesenchymal stem cell responses to hydrostatic pressure and shear stress, in: Eur Cell Mater, 2016, pp. 160-173.

[29] L.R. Stein, S.-i. Imai, The dynamic regulation of NAD metabolism in mitochondria, Trends Endocrinol Metab, 23 (2012) 420-428.

[30] A.S. Bause, M.C. Haigis, SIRT3 regulation of mitochondrial oxidative stress, Exp Gerontol, 48 (2013) 634-639.

[31] X. Yuan, Y. Liu, B. Bijonowski, A.C. Tsai, Q. Fu, T.M. Logan, T. Ma, Y. Li, NAD+/NADH Redox Alterations Reconfigure Metabolism and Rejuvenate Senescent Human Mesenchymal Stem Cells In Vitro, Commun Biol, 3 (2020) 774.

[32] Y.O. Mukhamedshina, O.A. Gracheva, D.M. Mukhutdinova, Y.A. Chelyshev, A.A. Rizvanov, Mesenchymal stem cells and the neuronal microenvironment in the area of spinal cord injury, Neural Regen Res, 14 (2019) 227-237.

[33] Z. Chen, L. Chen, C. Zeng, W.E. Wang, Functionally Improved Mesenchymal Stem Cells to Better Treat Myocardial Infarction, Stem Cells Int, 2018 (2018) 7045245.

[34] J. Hupfeld, I.H. Gorr, C. Schwald, N. Beaucamp, K. Wiechmann, K. Kuentzer, R. Huss, B. Rieger, M. Neubauer, H. Wegmeyer, Modulation of mesenchymal stromal cell characteristics by microcarrier culture in bioreactors, Biotechnol Bioeng, 111 (2014) 2290-2302.

[35] L.Y. Sun, D.K. Hsieh, W.S. Syu, Y.S. Li, H.T. Chiu, T.W. Chiou, Cell proliferation of human bone marrow mesenchymal stem cells on biodegradable microcarriers enhances in vitro differentiation potential, Cell Prolif, 43 (2010) 445-456.

[36] T.K.-P. Goh, Z.-Y. Zhang, A.K.-L. Chen, S. Reuveny, M. Choolani, J.K.Y. Chan, S.K.-W. Oh, Microcarrier culture for efficient expansion and osteogenic differentiation of human fetal mesenchymal stem cells, Biores Open Access, 2 (2013) 84-97.

[37] X. Yuan, T.M. Logan, T. Ma, Metabolism in Human Mesenchymal Stromal Cells: A Missing Link Between hMSC Biomanufacturing and Therapy?, Front Immunol, 10 (2019) 977.

[38] G. Higuera, D. Schop, F. Janssen, R. van Dijkhuizen-Radersma, T. van Boxtel, C.A. van Blitterswijk, Quantifying in vitro growth and metabolism kinetics of human mesenchymal stem cells using a mathematical model, Tissue Eng. Part A, 15 (2009) 2653-2663.

[39] D. Schop, F. Janssen, L. Rijn, H. Fernandes, R. Bloem, J. de Bruijn, R. Dijkhuizen-Radersma, Growth, Metabolism, and Growth Inhibitors of Mesenchymal Stem Cells, Tissue Eng. Part A, 15 (2009) 1877-1886.

[40] M.-Z. Ismadi, P. Gupta, A. Fouras, P. Verma, S. Jadhav, J. Bellare, K. Hourigan, Flow characterization of a spinner flask for induced pluripotent stem cell culture application, PLoS One, 9 (2014) e106493.

[41] W. Li, G. Ren, Y. Huang, J. Su, Y. Han, J. Li, X. Chen, K. Cao, Q. Chen, P. Shou, L. Zhang, Z.R. Yuan, A.I. Roberts, S. Shi, A.D. Le, Y. Shi, Mesenchymal stem cells: a double-edged sword in regulating immune responses, Cell Death Differ, 19 (2012) 1505-1513.

[42] M. Wang, Q. Yuan, L. Xie, Mesenchymal Stem Cell-Based Immunomodulation: Properties and Clinical Application, Stem Cells Int, 2018 (2018) 3057624.

[43] J.-P. Routy, B. Routy, G.M. Graziani, V. Mehraj, The Kynurenine Pathway Is a Double-Edged Sword in Immune-Privileged Sites and in Cancer: Implications for Immunotherapy, Int J Tryptophan Res, 9 (2016) 67-77.

[44] C. Huang, J. Dai, X.A. Zhang, Environmental physical cues determine the lineage specification of mesenchymal stem cells, Biochim Biophys Acta, 1850 (2015) 1261-1266.

[45] J. Lee, A.A. Abdeen, K.A. Kilian, Rewiring mesenchymal stem cell lineage specification by switching the biophysical microenvironment, Sci Rep 4 (2014) 5188.

[46] D. Li, Y. Han, Y. Zhuang, J. Fu, H. Liu, Q. Shi, X. Ju, Overexpression of COX-2 but not indoleamine 2,3-dioxygenase-1 enhances the immunosuppressive ability of human umbilical cord-derived mesenchymal stem cells, Int J Mol Med, 35 (2015) 1309-1316.

[47] H.J. Lee, M.F. Diaz, A. Ewere, S.D. Olson, C.S. Cox, Jr., P.L. Wenzel, Focal adhesion kinase signaling regulates anti-inflammatory function of bone marrow mesenchymal stromal cells induced by biomechanical force, Cell Signal, 38 (2017) 1-9.

[48] E. Fernandez-Rebollo, J. Franzen, R. Goetzke, J. Hollmann, A. Ostrowska, M. Oliverio, T. Sieben, B. Rath, J.W. Kornfeld, W. Wagner, Senescence-Associated Metabolomic Phenotype in Primary and iPSC-Derived Mesenchymal Stromal Cells, Stem Cell Reports, 14 (2020) 201-209.

[49] J.Q. Yin, J. Zhu, J.A. Ankrum, Manufacturing of primed mesenchymal stromal cells for therapy, Nat Biomed Eng, 3 (2019) 90-104.

[50] V. Turinetto, E. Vitale, C. Giachino, Senescence in Human Mesenchymal Stem Cells: Functional Changes and Implications in Stem Cell-Based Therapy, Int J Mol Sci, 17 (2016) 1164.

[51] E. Fouquerel, R.W. Sobol, ARTD1 (PARP1) activation and NAD(+) in DNA repair and cell death. DNA Repair (Amst), 23 (2014) 27-32.

[52] C. Cantó, K.J. Menzies, J. Auwerx, NAD(+) Metabolism and the Control of Energy Homeostasis: A Balancing Act between Mitochondria and the Nucleus, Cell Metab, 22 (2015) 31-53.

[53] J. Ge, L. Guo, S. Wang, Y. Zhang, T. Cai, R.C. Zhao, Y. Wu, The size of mesenchymal stem cells is a significant cause of vascular obstructions and stroke, Stem Cell Rev Rep, 10 (2014) 295-303.

[54] C.D.L. Folmes, P.P. Dzeja, T.J. Nelson, A. Terzic, Metabolic plasticity in stem cell homeostasis and differentiation, Cell Stem Cell, 11 (2012) 596-606.

[55] G.-J. Jeong, D. Kang, A.-K. Kim, K.-H. Han, H.R. Jeon, D.-I. Kim, Metabolites can regulate stem cell behavior through the STAT3/AKT pathway in a similar trend to that under hypoxic conditions, Sci Rep, 9 (2019) 6112.

[56] M. Barilani, R. Palorini, G. Votta, R. Piras, G. Buono, M. Grassi, V. Bollati, F. Chiaradonna, L. Lazzari, Central metabolism of functionally heterogeneous mesenchymal stromal cells, Sci Rep, 9 (2019) 15420.

List of Figures

Figure 1. Illustration of the microcarrier-based spinner flask platform for human mesenchymal stem cell (hMSC) expansion. (A) Spinner flask set-up on a programmable multi-position magnetic stirrer. (B) Zoom-in image of spinner flask and impeller. Intermittent agitation was used during inoculation period to maximize cell attachment to microcarriers. The spinner flasks were operated at 50-70 rpm.

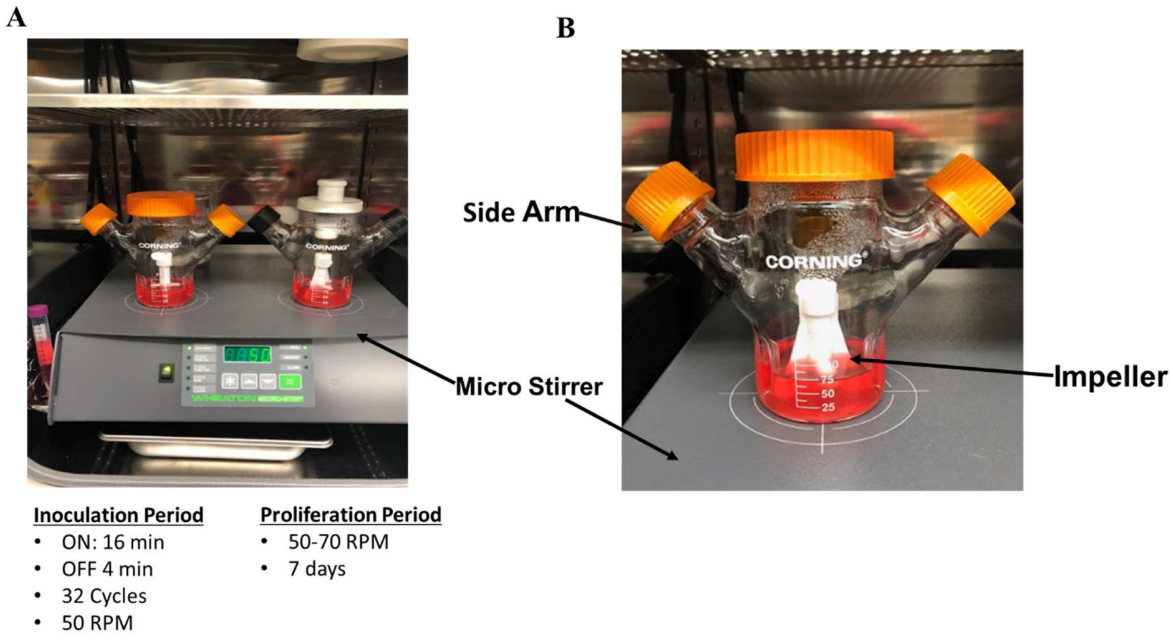

Figure 2. Effects of agitation speeds for BM-MSC expansion in microcarrier-based spinner flasks. (A) Hoechst-stained images of attached hMSCs on plastic plus microcarriers. Scale bar: 200 µm. (B) Cell number via DNA assay for cells from duplicate bioreactors agitated at 50 and 70 rpm over a 7-day culture. * indicates $p<0.05$. (C) Glucose and lactate concentration for a bioreactor run at 50 rpm, blue arrow indicates medium change right after sampling on day 4. (D) Lactate production to glucose consumption ratio (g/g) based on the concentration change. Groups labeled with * and groups labeled with # were compared in pair and shows significance with $p<0.05$.

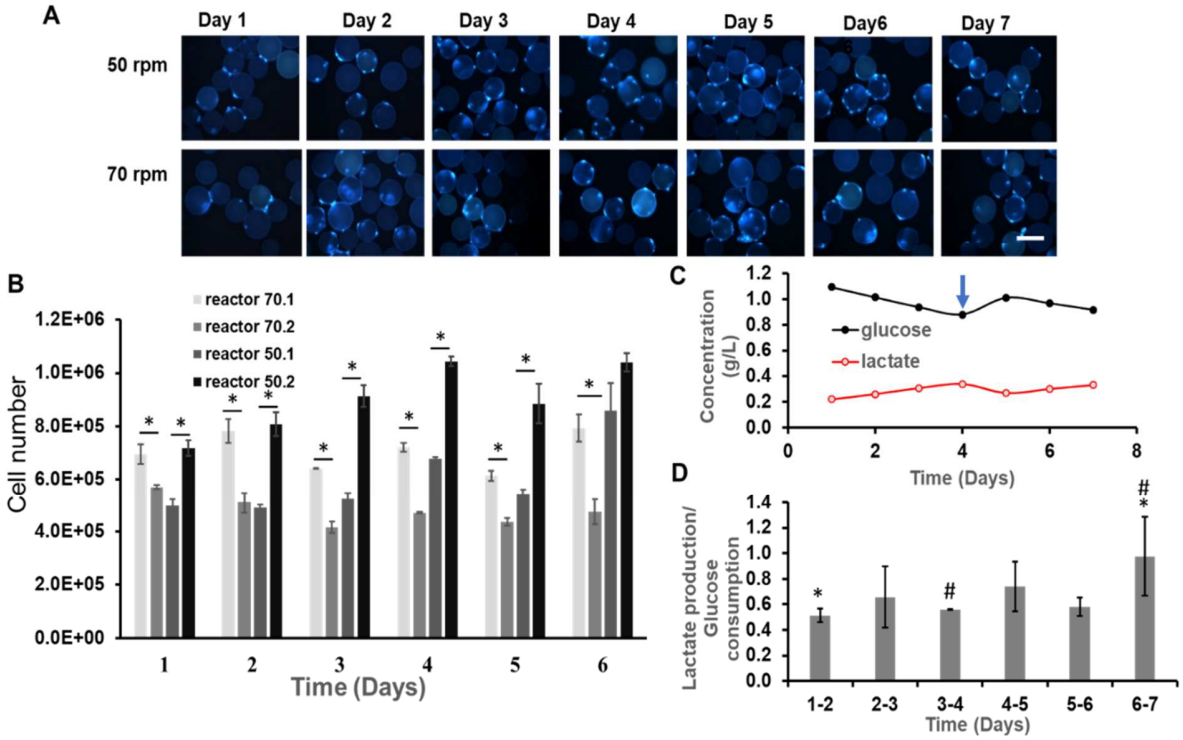

Figure 3. BM-MSC expansion in microcarrier-based spinner flasks at 50 rpm. (A) Hoechst-stained images of attached hMSCs on plastic plus microcarriers for a 7-day growth period. Te microcarriers were coated with fetal bovine serum (FBS). Scale bar: 200 µm. (B) Cell number via DNA assay for duplicate bioreactors agitated at 50 rpm over a 7-day culture period. * indicates $p<0.05$.

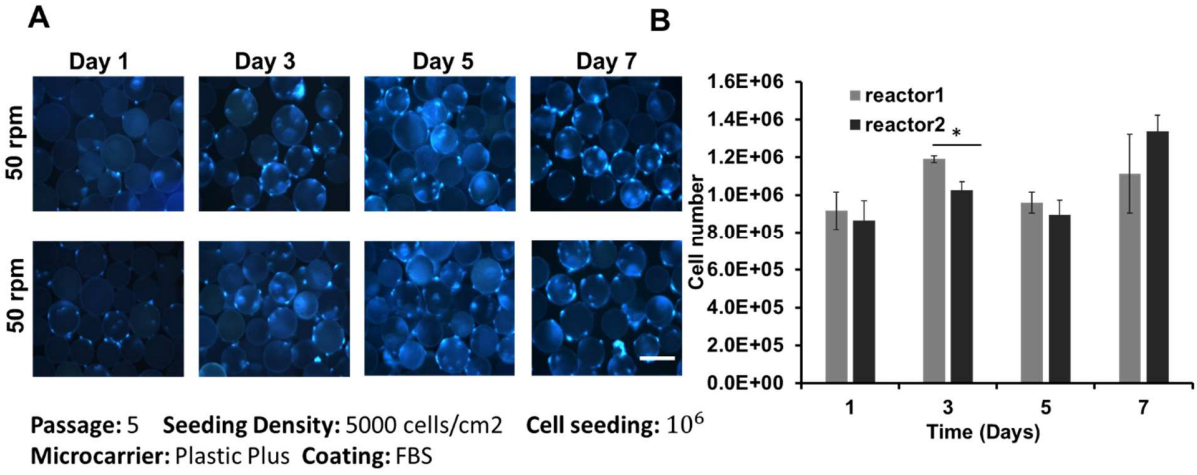

Figure 4. BM-MSC expansion in microcarrier-based spinner flasks at 70 rpm. (A). Hoechst-stained images of attached hMSCs on plastic plus microcarriers for a 7-day growth period. Scale bar: 200 µm. (B) MTT activity for duplicate bioreactors agitated at 70 rpm over a 7-day culture period. (C) Cell number via DNA assay for duplicate bioreactors agitated at 70 rpm over a 7-day culture period. * indicates $p<0.05$.

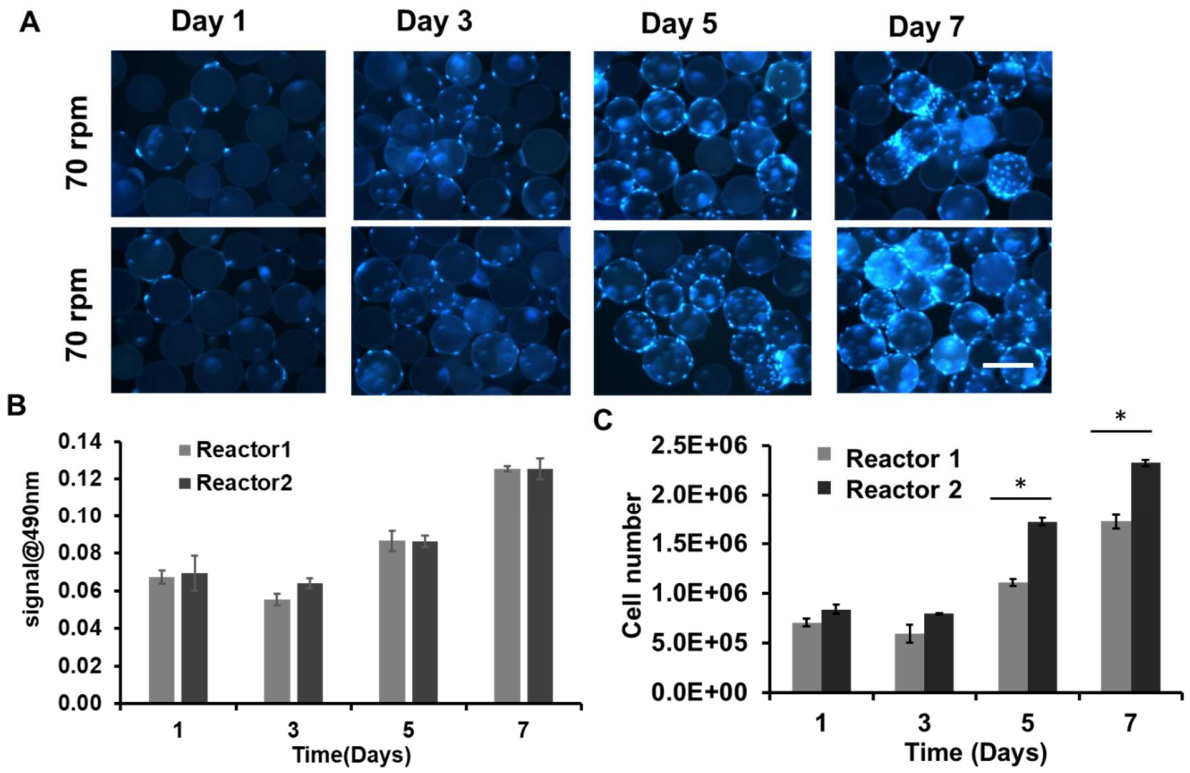

Figure 5. Agitation increases BM-MSC basal and IFNγ-induced immune response. IFNγ treatment induced the secretion of anti-inflammatory factors in hMSCs, i.e., indoleamine 2,3-dioxygenase (IDO) activity. (A) Kynurenine concentration for IFNγ treated and untreated hMSCs + microcarriers (MC) and hMSCs grown on planar culture. (B) Kynurenine concentration of IFNγ treated and untreated MC derived hMSCs allowed to adhere on a planar culture for two days and hMSCs grown on planar culture. * indicates $p<0.05$.

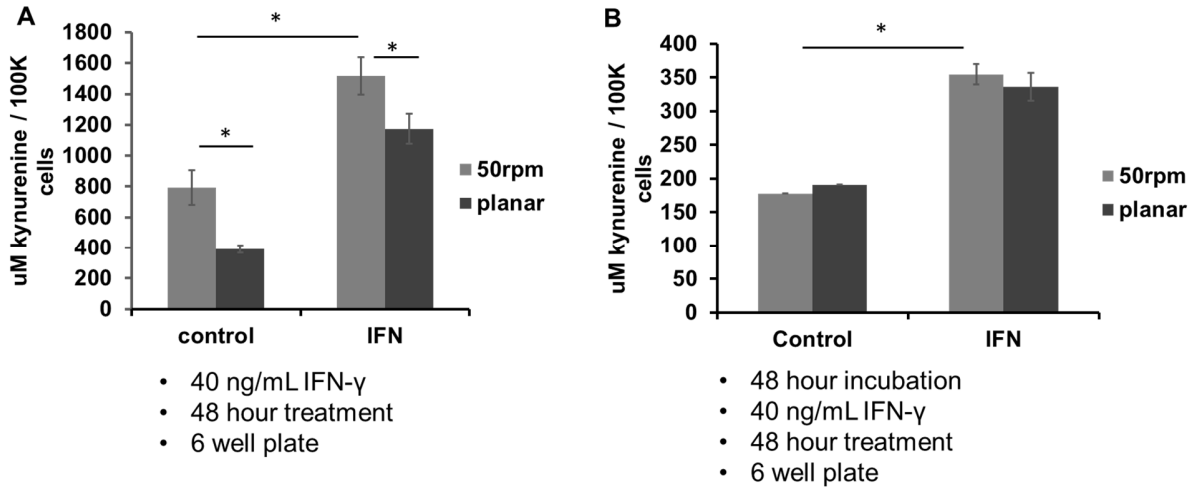

Figure 6. hASC expansion in microcarrier-based spinner flasks (50 rpm). (A). Hoechst-stained images of attached hASCs on plastic plus microcarriers for a 7-day growth period (Run 1). Run 1 was seeded at 0.7×10^6 total cells at day 1. Scale bar: 200 µm. (B) (i) Cell number via DNA assay over a 7-day culture period (Run 1), showing exponential growth. (ii) MTT activity over a 7-day culture period (Run 1). (C). Hoechst-stained images of attached hASCs for a 7-day growth period (Run 2), showing the plateau during day 5-7. Run 2 was seeded at 1.5×10^6 total cells at day 1. Scale bar: 200 µm. (D) (i) Cell number via DNA assay over a 7-day culture period (Run 2). (ii) MTT activity over a 7-day culture period (Run 2). * indicates $p<0.05$.

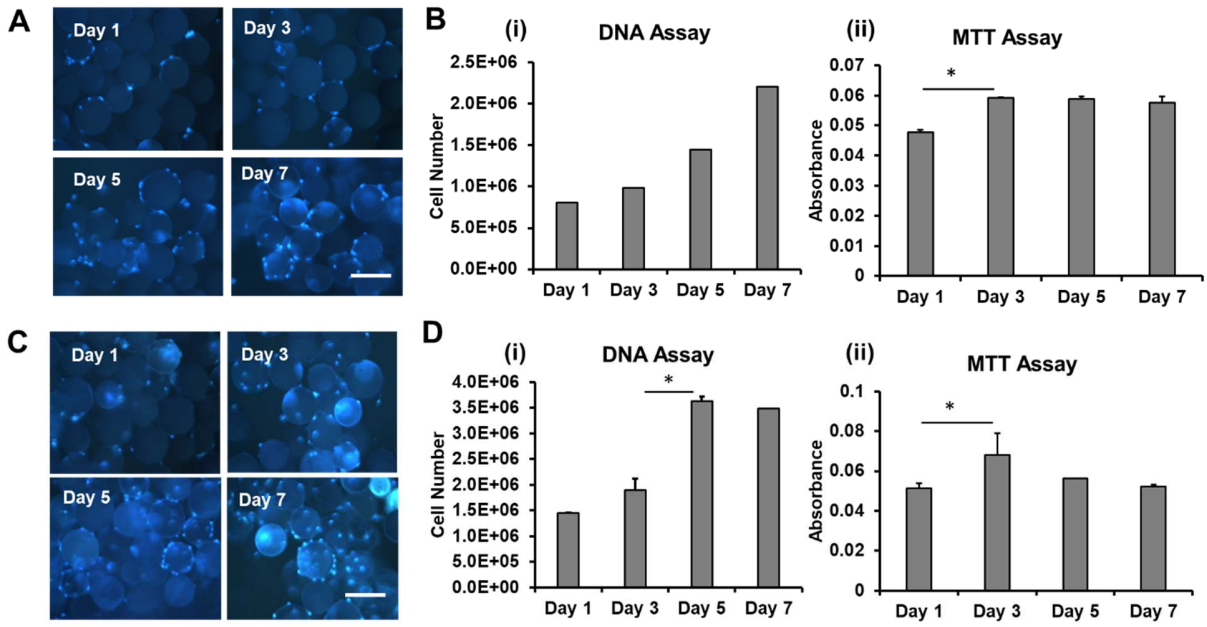

Figure 7. Metabolic characterization of hASCs expanded in microcarrier-based spinner flasks compared to planar culture. The agitation speed is 50 rpm. (A) NAD+/NADH ratio comparison; (B) Flow cytometry analysis of (i) Sirt1 and (ii) Sirt3 expression in hASCs. (C) Western blot analysis of Sirt1 protein expression. SFB: spinner flask bioreactor.

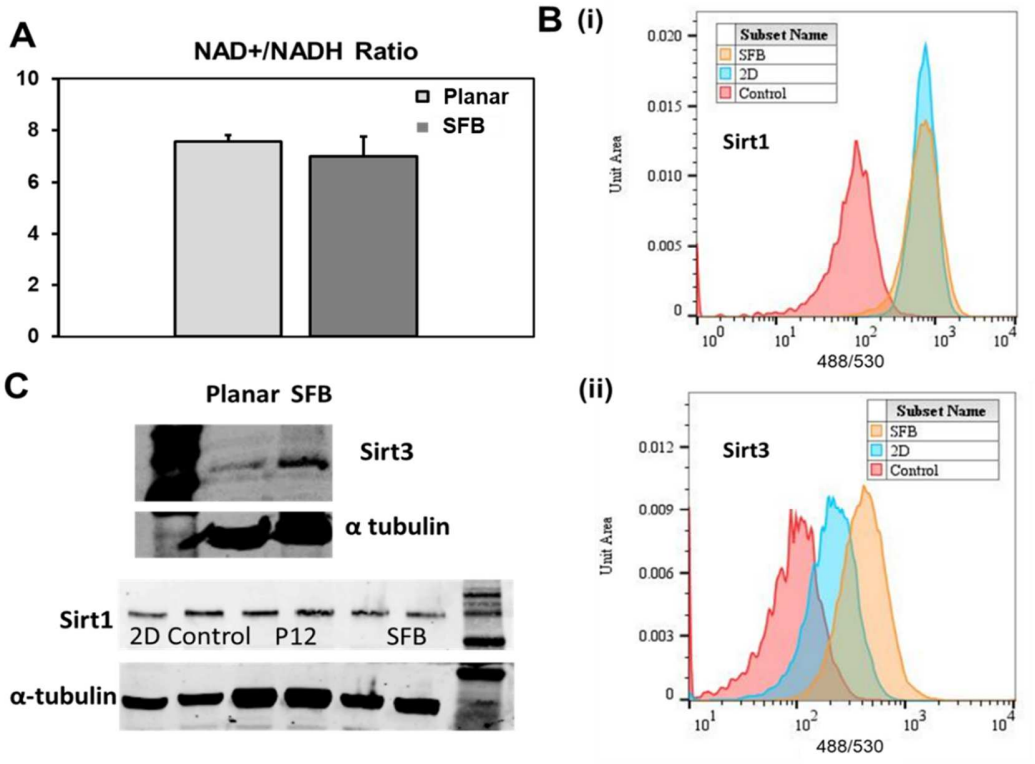

Figure 8. Physiological characterization of hASCs expanded in microcarrier-based spinner flasks compared to planar culture. The agitation speed is 50 rpm. (A) PGE2 secretion; (B) Kynurenine concentration (showing IDO activity) for IFNγ-treated and untreated hASCs+microcarriers (MC) and hASCs grown on planar culture. (C) Flow cytometry analysis of reactive oxygen species (ROS) production. (D) Forward scatter vs side scatter by flow cytometry to show cell size differences. SFB: spinner flask bioreactor. * indicates $p<0.05$.